UC Irvine
UC Irvine Previously Published Works

Title
Radiacoustic imaging (RAI) of spatially fractionated proton therapy in human torso phantom and in vivo

Permalink
https://escholarship.org/uc/item/15b8h4t7

Journal
Progress in Biomedical Optics and Imaging, 13931

ISSN
1605-7422

ISBN
978-1-5106-9799-7

Authors
Bjegovic, K
Pandey, PK
Gonzalez, G
et al.

Publication Date
2026

DOI
10.1117/12.3087778

Copyright Information
This work is made available under the terms of a Creative Commons Attribution License, available at https://creativecommons.org/licenses/by/4.0/

eScholarship.org Powered by the California Digital Library
University of California

Radiacoustic Imaging (RAI) of Spatially Fractionated Proton Therapy in Human Torso Phantom and in vivo

K. Bjegovic[a], P.K. Pandey[a], G. Gonzalez[b], L. Rodriguez-Gonzalez[a], P. M. Budhrani[b], M. Roper[b], Y. Chen[b], and L. Xiang[a,c,d]

[a]Department of Biomedical Engineering, University of California, Irvine, CA 92617, USA
[b]Department of Radiation Oncology, University of Oklahoma Health Sciences Center, Oklahoma City, OK, 73104, United States of America
[c]Department of Radiological Sciences, University of California at Irvine, Irvine, CA 92697, United States of America
[d]Beckman Laser Institute Medical Clinic, University of California, Irvine, Irvine, CA 92612, United States of America

ABSTRACT

Proton therapy monitoring is currently limited to surface dosimetry despite the need for in vivo Bragg peak localization and monitoring of more complex delivery paradigms such as spatially fractionated GRID therapy, both of which are associated with improved patient outcomes. Radiacoustic imaging (RAI), which captures acoustic waves generated by pulsed proton dose deposition deep within the body, enables pulse-resolved, volumetric, quantitative monitoring of Bragg peak location and total dose delivery. In this work, the livers of a human torso phantom and a rabbit were irradiated with spatially separated proton beams, and the resulting radiacoustic signals were reconstructed into volumetric dose maps spanning both individual pulses and entire treatments. These high-fidelity reconstructions demonstrate the potential of RAI to enable adaptive radiotherapy and to ensure accurate in vivo delivery of spatially fractionated proton therapies.

Keywords: Radioacoustic imaging, in vivo dosimetry, GRID therapy, Protoacoustics, Proton Therapy, SFRT

1. INTRODUCTION

Radiotherapy, delivered to almost two-thirds of all cancer patients in the United States,[1] results in side effects ranging from skin toxicity to loss of function in radiosensitive normal tissues such as the gastrointestinal tract, as photons deposit dose before, within, and beyond the tumor volume as they traverse the patient's body.[2–5] In an effort to reduce dose delivered to normal tissue, the clinical standard of care is shifting toward proton therapy, which deposits dose in a Bragg peak (BP) depth profile. While the dose delivered prior to the tumor region is similar to that of photon therapy, minimal dose is delivered distal to the tumor, as protons have a finite range and a significantly different stopping power compared to photons.[6,7] Treatment plans are therefore generated to select beam angles that minimize traversal through radiosensitive tissues proximal to the tumor volume. Although Bragg peak delivery is the greatest advantage of proton therapy, it also poses a significant challenge: the lack of in-line dosimetry.[8] Photon therapy is commonly monitored in the clinic using electronic portal imaging devices (EPIDs), which generate a differential two-dimensional dose map by comparing the incident beam to the signal measured by a planar ionization chamber that captures photons exiting the patient.[9,10] In contrast, protons do not exit the body, resulting in no direct verification of spatially resolved dose deposition or Bragg peak location. Consequently, substantial doses are delivered proximal to and at the BP within the body, with dose distributions inferred from Monte Carlo simulations based on prior patient CT data.[11]

Further author information: (Send correspondence to L. Xiang)
L. Xiang: liangzhx@hs.uci.edu
Y. Chen: yong-chen@ouhsc.edu

Medical Imaging 2026: Ultrasonic Imaging and Tomography, edited by Christian Boehm, Mohammad Mehrmohammadi, Shawn Liangzhong Xiang, Proc. of SPIE Vol. 13931, 139310E · 2026 Published by SPIE
1605-7422 · doi: 10.1117/12.3087778

To further reduce dose delivered proximal to the planned target volume (PTV), spatially fractionated delivery techniques such as GRID therapy have gained clinical interest. These delivery schemes create large unirradiated regions between beamlets, resulting in reduced dose to normal tissue proximal to the PTV compared to conventional irradiation schemes. As the protons scatter and overlap within the body approaching the PTV, a more homogeneous dose distribution is formed at the Bragg peak, enabling maintained tumor control.[12,13] Such delivery paradigms place even greater importance on in vivo monitoring, as both the peak-to-valley dose structure and the resulting homogeneous dose within the PTV must be verified.[14,15]

Current gold-standard dosimeters used in proton therapy include Gafchromic films, which provide two-dimensional surface dosimetry of the entire treatment but must be digitized approximately 24 hours post-irradiation,[16,17] and ionization chambers, which monitor the beam prior to entry into the body.[18,19] This lack of real-time, pulse-resolved, volumetric dosimetry motivates the development of emerging monitoring techniques such as radiacoustic imaging (RAI). RAI exploits acoustic waves generated by pulsed radiation beams; as energy is deposited, a localized temperature rise produces a rapid pressure increase that launches spherical acoustic waves, the amplitudes of which encode dose information.[20,21] By detecting these radiacoustic (RA) signals with multiple ultrasound transducers, the spatial distribution of dose deposited in tissue can be reconstructed on a single-pulse scale.[22–25]

In this work, we demonstrate radiacoustic imaging (RAI) as a real-time, pulse-resolved, volumetric dosimetry technique for monitoring spatially fractionated proton therapy. We present three-dimensional RAI reconstructions of proton dose deposition during GRID-style beam deliveries in both a human torso phantom and in vivo in a rabbit model. Using a clinical proton therapy system and treatment plans generated in a commercial treatment planning system, we show that RAI can localize the Bragg peak and resolve individual beam spots as well as cumulative dose distributions across an entire treatment. These results highlight the capability of RAI to monitor complex proton delivery paradigms in heterogeneous media and represent an important step toward in vivo verification and adaptive monitoring of spatially fractionated proton therapies.

2. METHODS

A clinical proton beamline (Mevion, USA) was used to deliver proton beams of varying location and delivered charge to a human torso phantom (TruePhantom, Canada) and in vivo to a female New Zealand White rabbit under an IACUC-approved protocol (insert protocol number). Both the human torso phantom and the rabbit underwent CT imaging prior to irradiation, and treatment plans targeting the liver were generated in RayStation, a clinical treatment planning software that enables complex, optimized planning. The human torso phantom received proton beams with a beam width of 2.3 cm at the Bragg peak (BP) delivered to four locations within the liver, with 3 cm spacing between beam centers, as shown in Fig. 1b. In the rabbit experiments, proton beams were delivered to two locations (Fig. 2b–c), reflecting the smaller size of the rabbit liver.

Radiacoustic signals were acquired using a custom 256-element matrix ultrasound array mounted on a robotic arm (UFactory, China) to provide mechanical stability and enable precise positioning during beam delivery (Fig. 1a). The array was connected to a custom 256-channel parallel preamplifier and data acquisition system (Photosound, USA). The transducer was aligned to be perpendicular to and centered on the beam axis using CT-visible markers and the clinical laser alignment system typically employed for patient setup. All radiacoustic (RA) signals collected in the human torso phantom were processed in MATLAB and reconstructed using a universal back-projection algorithm.

For phantom experiments, the matrix array was directly coupled to the torso phantom using ultrasound gel, with the phantom positioned supine on the treatment couch (Fig. 1a). Beam delivery was synchronized with the data acquisition system using a scintillator placed in the beam path. While the experimental protocols for phantom and in vivo studies were similar, several important differences were required. For in vivo experiments, the rabbit was anesthetized and denuded; however, the smaller surface area and increased curvature of the abdomen and back posed challenges for direct transducer coupling. To address this, the transducer array was placed in a water bath with a deformable membrane, allowing it to conform to the rabbit's anatomy. The membrane was coupled to the denuded skin using ultrasound gel (Fig. 2a). Due to the presence of air pockets in the stomach located superior to the liver, the rabbit was positioned prone to provide an improved acoustic

window for RAI. Additionally, phantom experiments indicated that placement of the scintillator in the beam path influenced beam shape and Bragg peak location. Therefore, for in vivo experiments, synchronization was achieved using a neutron detector (DoseOptics, USA) positioned lateral to the rabbit, ensuring that beam delivery was not perturbed.

RAI signal reconstruction for these experiments was performed using a multi-stage pipeline. Acquired signals were first denoised using a learned denoising network, followed by initial image formation using a conventional time-reversal reconstruction algorithm. The resulting volumes were then refined using a physics-informed neural network (PINN) to mitigate limited-angle artifacts, enabling reconstruction of the full distal proton dose tail that cannot be fully recovered using time-reversal methods alone. The reconstruction methodology, including network architecture, training strategy, and physics-based constraints, is described in detail in a recently published study.[26]

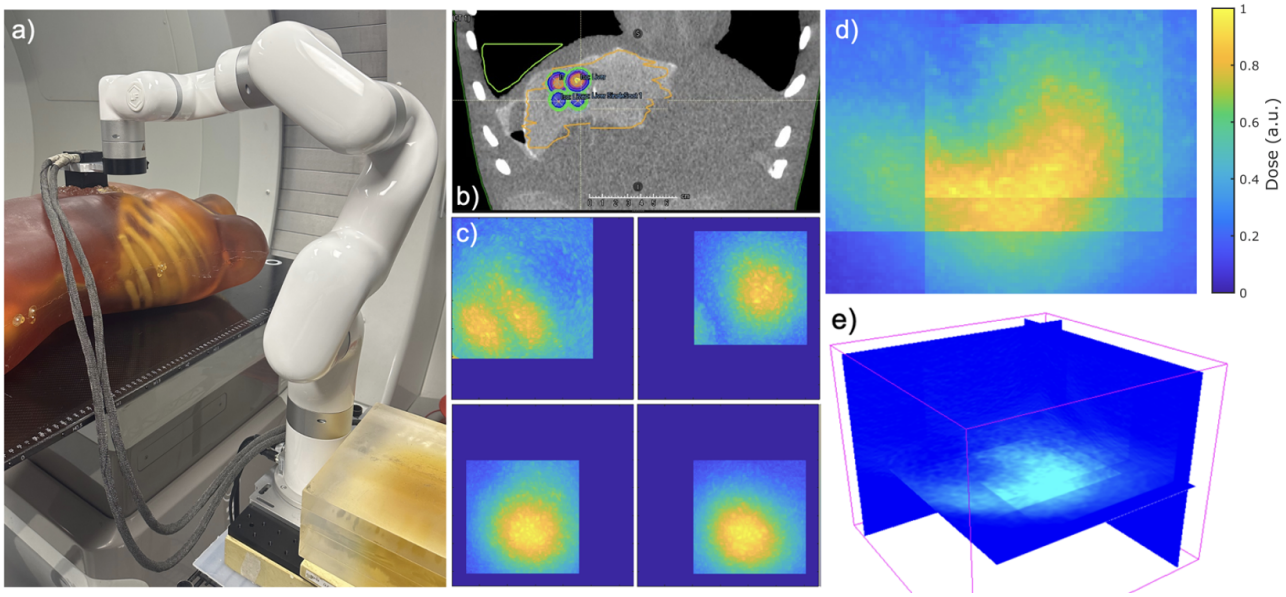

Figure 1. Three-dimensional RAI monitoring of GRID proton therapy in a human torso phantom. (a) The clinical setup, with the xARM6 robotic arm securing the matrix array to a human torso phantom on the patient couch of the Mevion Proton Therapy System. (b) A CT scan of the human torso phantom used in the treatment planning system (TPS) to select four pseudo-tumors within the liver and determine the proton beam energy. (c) X–Y dose distributions of the four individual beam spots reconstructed in MATLAB. (d) The combined X–Y dose distribution resulting from treatment with the four spots. (e) Three-dimensional RAI dose deposition monitoring, illustrating the Bragg peak depth and spatial dose conformity throughout the human torso phantom.

3. RESULTS

The results obtained in the human torso phantom for radiacoustic monitoring of GRID proton therapy are presented in Fig. 1. Figure 1b shows the GRID delivery geometry overlaid on the CT-based treatment plan, while Fig. 1c presents the reconstructed dose distributions of the individual beam spots in the same X–Y plane. The cumulative dose distribution is shown in Fig. 1d in the X–Y plane and volumetrically in Fig. 1e, demonstrating the ability of radiacoustic imaging (RAI) to monitor proton therapy delivery in a complex, heterogeneous medium. Three of the four beam spots (upper right, bottom-left, and bottom-right) exhibit clearly defined Bragg peak cross-sections. In contrast, the top-left beam spot is partially obscured by the rib cage, resulting in a degraded acoustic window between the Bragg peak in the liver and the transducer. This limitation may be mitigated by positioning the transducer at a more favorable location or by tilting the transducer using a water-filled membrane rather than directly coupling to the body surface. Figure 3 presents an analysis

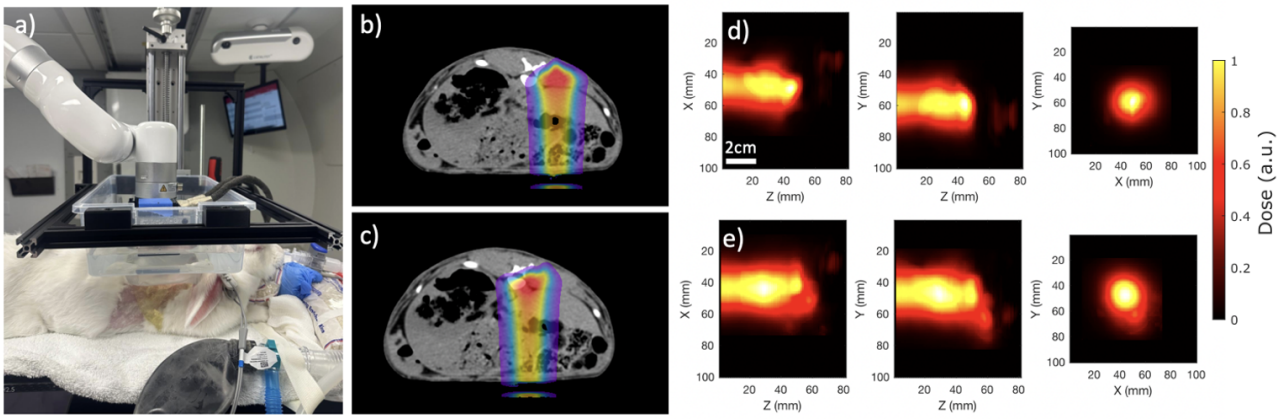

Figure 2. In vivo RAI dose monitoring during proton beam delivery in a rabbit model. (a) Experimental setup showing a water bath coupled to the posterior side of a denuded rabbit, positioned using a robotic arm for in vivo proton beam delivery. The rabbit was anesthetized and continuously monitored throughout treatment. (b–c) RayStation treatment plans depicting two proton beam spot deliveries within the rabbit liver. (d–e) RAI dose maps corresponding to the two beams, illustrating the Bragg peak (BP) depth–dose profile and cross-sectional dose distributions in all three anatomical planes.

of the axial and lateral spatial resolution using a representative reconstruction of the bottom-right beam spot; Gaussian fitting yielded an axial resolution of 1.8 mm and a lateral resolution of 2.67 cm.

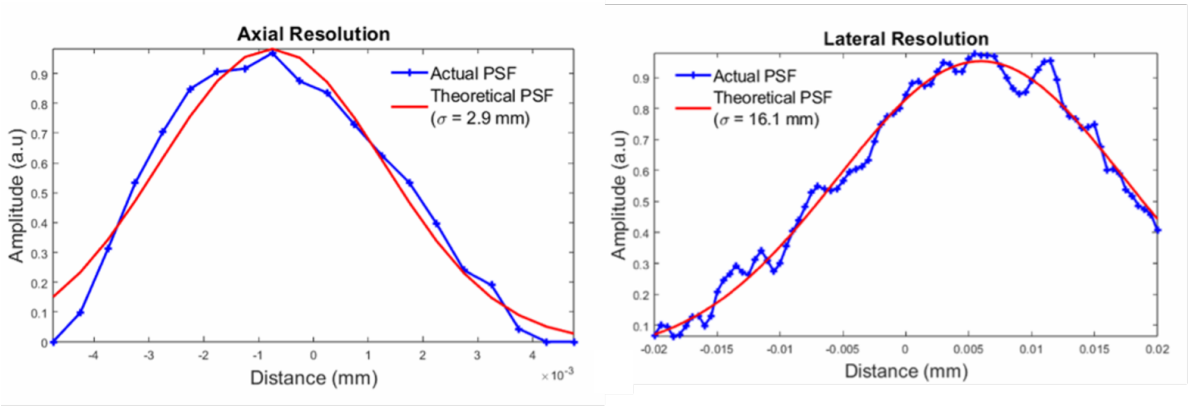

Figure 3. Point spread function and spatial resolution of RAI beam deposition. The graph shows the point spread function (PSF) of the beam deposition in the Y–Z plane obtained from the averaged signal. The measured PSF is shown alongside a Gaussian fit, demonstrating an axial resolution of 4.8 mm and a lateral resolution of 2.67 cm.

Finally, the in vivo rabbit delivery results are presented in Fig. 2. The two proton beam spots delivered to the rabbit liver are shown in Fig. 2b and 2c, with a reduced center-to-center spacing of 1 cm reflecting the size constraints of the rabbit liver. The corresponding in vivo radiacoustic reconstructions are shown in Fig. 2d and 2e. In the Y–Z plane, the reconstructed Bragg peak depth–dose profiles closely match the treatment plans, while in the X–Y plane the reconstructed beam cross-sections agree well with the expected beam shape and size. In contrast to the human torso phantom, which exhibited well-defined and symmetric beam shapes, the in vivo treatment plans and corresponding RAI reconstructions show distorted Bragg peak profiles due to the presence of bone and air. Anatomical differences between humans and rabbits, together with the smaller size of the rabbit anatomy, limited the ability to generate treatment plans that fully avoided bony structures and heterogeneous air pockets in the stomach. The effects of proton interactions with these heterogeneities are

evident in both the simulated and reconstructed beam shapes. Future work will aim to improve reconstruction accuracy by incorporating heterogeneous speed-of-sound information derived from CT and by leveraging dual-modality ultrasound imaging to mitigate the effects of respiratory motion, which can lead to motion-induced blurring and inaccuracies in Bragg peak localization during in vivo imaging.

4. CONCLUSION

In conclusion, radiacoustic imaging (RAI) shows substantial promise as a real-time, in vivo modality for monitoring proton dose deposition, addressing a critical limitation in current proton therapy verification. The ability to generate pulse-resolved, volumetric dose maps establishes RAI as a powerful tool for treatment verification and lays the groundwork for future adaptive proton radiotherapy. This study provides the first demonstration of RAI-based monitoring of spatially fractionated GRID proton therapy and the first in vivo demonstration of radiacoustic dose mapping during proton beam delivery. To our knowledge, no previous studies have achieved in vivo RAI monitoring of proton therapy, and these results represent a meaningful step toward clinical implementation and patient translation of radiacoustic-based proton therapy monitoring.

5. ACKNOWLEDGEMENT

This work was supported by the National Institutes of Health (R37CA240806, U01CA288351, R50CA283816). The authors would like to acknowledge the support from UCI Chao Family Comprehensive Cancer Center (No. P30CA062203).

6. CONFLICT OF INTEREST

Liangzhong Xiang has financial interest in SoundDose, Inc., which, however, did not support this work. The remaining authors declare no conflict of interests.

REFERENCES

[1] Schaue, D. and McBride, W. H., "Opportunities and challenges of radiotherapy for treating cancer," *Nature reviews Clinical oncology* **12**(9), 527–540 (2015).

[2] Chen, G., Han, Y., Zhang, H., Tu, W., and Zhang, S., "Radiotherapy-induced digestive injury: diagnosis, treatment and mechanisms," *Frontiers in oncology* **11**, 757973 (2021).

[3] Yu, Z., Xu, C., Song, B., Zhang, S., Chen, C., Li, C., and Zhang, S., "Tissue fibrosis induced by radiotherapy: current understanding of the molecular mechanisms, diagnosis and therapeutic advances," *Journal of translational medicine* **21**(1), 708 (2023).

[4] Bray, F. N., Simmons, B. J., Wolfson, A. H., and Nouri, K., "Acute and chronic cutaneous reactions to ionizing radiation therapy," *Dermatology and therapy* **6**(2), 185–206 (2016).

[5] He, Y., Wang, M., Gao, C., Hao, Y., He, S., and Li, L., "Incidence, risk factors, and management of radiotherapy-related skin toxicity in rectoanal cancer patients: a systematic review and meta-analysis," *Journal of Gastrointestinal Cancer* **57**(1), 16 (2026).

[6] Newhauser, W. D. and Zhang, R., "The physics of proton therapy," *Physics in Medicine & Biology* **60**(8), R155 (2015).

[7] Mohan, R. and Grosshans, D., "Proton therapy–present and future," *Advanced drug delivery reviews* **109**, 26–44 (2017).

[8] Poon, D. M., Wu, S., Ho, L., Cheung, K. Y., and Yu, B., "Proton therapy for prostate cancer: challenges and opportunities," *Cancers* **14**(4), 925 (2022).

[9] Nailon, W. H., Welsh, D., McDonald, K., Burns, D., Forsyth, J., Cooke, G., Cutanda, F., Carruthers, L. J., McLaren, D. B., Puxeu Vaqué, J., et al., "Epid-based in vivo dosimetry using dosimetry check™: overview and clinical experience in a 5-yr study including breast, lung, prostate, and head and neck cancer patients," *Journal of Applied Clinical Medical Physics* **20**(1), 6–16 (2019).

[10] Olaciregui-Ruiz, I., Beddar, S., Greer, P., Jornet, N., McCurdy, B., Paiva-Fonseca, G., Mijnheer, B., and Verhaegen, F., "In vivo dosimetry in external beam photon radiotherapy: Requirements and future directions for research, development, and clinical practice," *Physics and imaging in radiation oncology* **15**, 108–116 (2020).

[11] Paganetti, H., Botas, P., Sharp, G. C., and Winey, B., "Adaptive proton therapy," *Physics in Medicine & Biology* **66**(22), 22TR01 (2021).

[12] Mohiuddin, M., Lynch, C., Gao, M., and Hartsell, W., "Early clinical results of proton spatially fractionated grid radiation therapy (sfgrt)," *The British Journal of Radiology* **93**(1107), 20190572 (2020).

[13] Peñagarícano, J. A., Moros, E. G., Ratanatharathorn, V., Yan, Y., and Corry, P., "Evaluation of spatially fractionated radiotherapy (grid) and definitive chemoradiotherapy with curative intent for locally advanced squamous cell carcinoma of the head and neck: initial response rates and toxicity," *International Journal of Radiation Oncology* Biology* Physics* **76**(5), 1369–1375 (2010).

[14] Paganetti, H., Beltran, C., Both, S., Dong, L., Flanz, J., Furutani, K., Grassberger, C., Grosshans, D. R., Knopf, A.-C., Langendijk, J. A., et al., "Roadmap: proton therapy physics and biology," *Physics in Medicine & Biology* **66**(5), 05RM01 (2021).

[15] Klimpki, G., Eichin, M., Bula, C., Rechsteiner, U., Psoroulas, S., Weber, D., Lomax, A., and Meer, D., "Real-time beam monitoring in scanned proton therapy," *Nuclear Instruments and Methods in Physics Research Section A: Accelerators, Spectrometers, Detectors and Associated Equipment* **891**, 62–67 (2018).

[16] Yeo, I. J., Teran, A., Ghebremedhin, A., Johnson, M., and Patyal, B., "Radiographic film dosimetry of proton beams for depth-dose constancy check and beam profile measurement," *Journal of Applied Clinical Medical Physics* **16**(3), 318–328 (2015).

[17] Kern, A., Bäumer, C., Kröninger, K., Mertens, L., Timmermann, B., Walbersloh, J., and Wulff, J., "Determination of surface dose in pencil beam scanning proton therapy," *Medical Physics* **47**(5), 2277–2288 (2020).

[18] Lee, E., Lourenço, A. M., Speth, J., Lee, N., Subiel, A., Romano, F., Thomas, R., Amos, R. A., Zhang, Y., Xiao, Z., et al., "Ultrahigh dose rate pencil beam scanning proton dosimetry using ion chambers and a calorimeter in support of first in-human flash clinical trial," *Medical Physics* **49**(9), 6171–6182 (2022).

[19] Liu, K., Holmes, S., Hooten, B., Schüler, E., and Beddar, S., "Evaluation of ion chamber response for applications in electron flash radiotherapy," *Medical physics* **51**(1), 494–508 (2024).

[20] Xu, Y. and Xiang, S. L., "Radiacoustic imaging," *Nature Reviews Physics* **7**(11), 660–670 (2025).

[21] Hayakawa, Y., Tada, J., Arai, N., Hosono, K., Sato, M., Wagai, T., Tsuji, H., and Tsujii, H., "Acoustic pulse generated in a patient during treatment by pulsed proton radiation beam," *Radiation Oncology Investigations* **3**(1), 42–45 (1995).

[22] Wang, S., Gonzalez, G., Sun, L., Xu, Y., Pandey, P., Chen, Y., and Xiang, S., "Real-time tracking of the bragg peak during proton therapy via 3d protoacoustic imaging in a clinical scenario," *npj Imaging* **2**(1), 34 (2024).

[23] Yu, Y., Qi, P., and Peng, H., "Feasibility study of 3d time-reversal reconstruction of proton-induced acoustic signals for dose verification in the head and the liver: A simulation study," *Medical physics* **48**(8), 4485–4497 (2021).

[24] Bjegovic, K., Ren, L., Chen, Y., Schüler, E., Xing, L., and Xiang, S., "Seeing the invisible: In vivo dosimetry in radiotherapy with radiacoustic imaging," *Medical physics* **52**(12), e70165 (2025).

[25] Schauer, J., Wieser, H.-P., Huang, Y., Ruser, H., Lascaud, J., Würl, M., Chmyrov, A., Vidal, M., Herault, J., Ntziachristos, V., et al., "Proton beam range verification by means of ionoacoustic measurements at clinically relevant doses using a correlation-based evaluation," *Frontiers in Oncology* **12**, 925542 (2022).

[26] SUN, L., Bjegovic, K., Rodriguez-Gonzalez, L., Xu, Y., Yan, Y., Gonzalez, G., Whitmore, L., Connell, L., Lang, Y., Pandey, P., et al., "A physics-informed neural network for in vivo dosimetry using quantitative radiacoustic imaging," (2026).